Research Article

Aibi research, management and engineering journal. Volume 13, Number 2, Pag 1-11, May - August 2025, ISSN 2346-030X

Novel control method for DC microgrid based on hybrid renewable power sources with multiport DC to DC converter

Miguel Mateo Puma-Chávez[1]
[1]*Universidad Continental, Arequipa - Perú*

Received: november 29, 2024.
Accepted: april 26, 2025.
Publicado: may 01, 2025.

***Abstract*—** Power supply systems built upon multiple renewable energy sources can provide reliable power. By using an efficient control method along with suitable converters can improve the power quality as well as can be able to supply stable power to various loads. Multiple renewable sources connected to DC-Microgrid are becoming popular and require an efficient control method to make both energy management as well as maintain power quality at load bus. Since many renewable energy-based power generating units, battery bank and loads are connected, a multiport DC to DC converter is selected in this paper. Solar plant, wind power plant, hydrogen-based power units (AE and FC) and battery bank are connected to a common DC bus. A novel control unit is developed in this paper on multiport DC to DC circuit to maintain both energy management system as well as constant voltage at DC bus. Super twisting sliding mode controllers are used in the proposed control methodology to improve the performance of proposed system under rapid changes in the system including wind speed, solar irradiance and load current. Hardware - in the - Loop is developed by using OPAL-RT modules to present various results under different operating conditions.

Keywords: super twisting sliding mode, multiport converter, hardware in the loop, renewable energy sources.

*Corresponding author: miguel.puma@tesla.org.pe (Miguel Mateo Puma Chávez).
Peer reviewing is a responsability of the Universidad de Santander.
How to cite this article: M. M. Puma-Chávez, “Novel control method for DC microgrid based on hybrid renewable power sources with multiport DC to DC converter”, *Aibi research, management and engineering journal*, vol. 13, no. 2, pp. 1-11 2025, doi: 10.15649/2346030X.4076

I. INTRODUCTION

Electric power supply systems powered by RESs are becoming famous and establishing at many places worldwide [1], [12]. Among many, SPP and WPP are major power production units at many places. Generally, PVS are used to generate electrical power from solar irradiance. Permanent magnet synchronous generators are used to generate electrical supply through mechanical power of wind turbines for medium power applications [13], [14]. Nevertheless, multiple converters are required to integrate all these power sources into a common DC bus. Moreover, both wind speed and solar irradiances are depending on nature and even there is no irradiance during night and cloudy days. Hence, energy storage modules like batteries must be integrated to the power supply system to maintain EMS [15]. However, batteries require regular maintenance and required replacements since having only few years of lifetime [16]-[19]. Therefore, hydrogen-based energy storage devices are considered in this paper. An AE is used to produce hydrogen when there is high power generation than load and FC is used to produce electricity by using stored hydrogen and oxygen during high load demand than generation.

In general, DCMG is popular and established at many places worldwide. Hence, a DCMG is established by integrating SPP, WPP, AE, FC, Battery bank and various loads. Normally, many converters are required to integrate all these comments to establish a DC bus [20], [21]. There will be an option to interconnect DCMG to AC Microgrid by using an inverter with an appropriate control model. In this paper, a multiport DC to DC circuit is selected and connected all components to DC bus through this multiport DC to DC converter. Among many controllers, STSM controller can be able to produce accurate output under rapid variations in the DCMG under various operating conditions. Therefore, STSM controllers are used while designing the control methodology for the multiport DC to DC circuit [2]. The proposed control method of the multiport converter includes the operation of MPPTs of wind turbine and PVS under variations in wind speed and solar irradiances respectively, operation coordination among battery bank, AE and FC by regulating voltage at DC bus effectively. Hence, a common control methodology is proposed to drive the multiport DC to DC convert to perform various tasks.

Various DC loads can be connected at DC bus by using their respective converting devices, hence a constant voltage at DC bus must be produced by using proposed control methodology. The rest of the paper is organized by incorporating details about DCMG in Section-II, modeling of various components in Section-III, proposed control methodology along with STSM controllers in Section-IV. Results based on HIL under various operating conditions are presented in Section-V and conclusion prepared in Section-VI.

II. OVERVIEW OF DCMG

A simple layout of various components connected to DCMG is depicted in Fig. 1 by using multiport converter. The EMS must be developed among all components integrated to establish a DCMG to manage energy flow. There will be an option to connect AC Microgrid by using simple DC to AC converter (i.e., an inverter). A detailed connection (generalized block diagram) among various components along with their respective converters is depicted in Fig. 2, is a commonly existing network of a DCMG powered by various RESs based power production units. Authors in [3] proposed a hierarchical control method for super capacitor based DCMG. Power processing of RESs based DCMG is developed by authors in [4]. High efficiency DC to DC converters are designed by authors in [5] for RESs powered DCMG. Significance of battery energy storage in DCMG and control strategy is proposed for protection by authors in [6]. Authors in [7] presented high gains DC to DC converters for DCMGs. Control and design of DCMG is discussed by authors in [8]. A smooth operation of standalone DCMG is developed by authors in [9] under high and low penetration of RESs. However, author [3-9] did not consider multiport DC to DC converter as well as STSM controllers in their control methodologies.

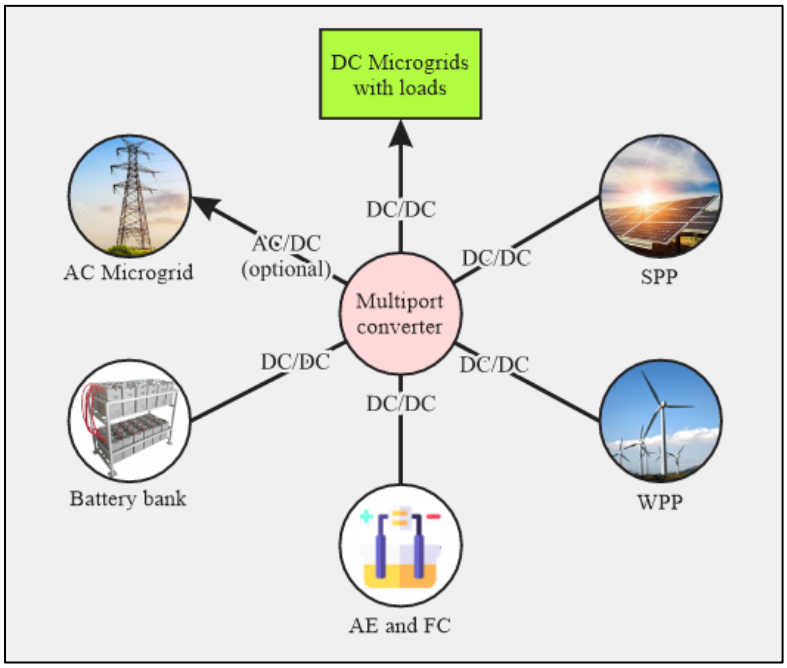

Figure 1: Layout of DCMG with multiport converter.
Source: Own elaboration.

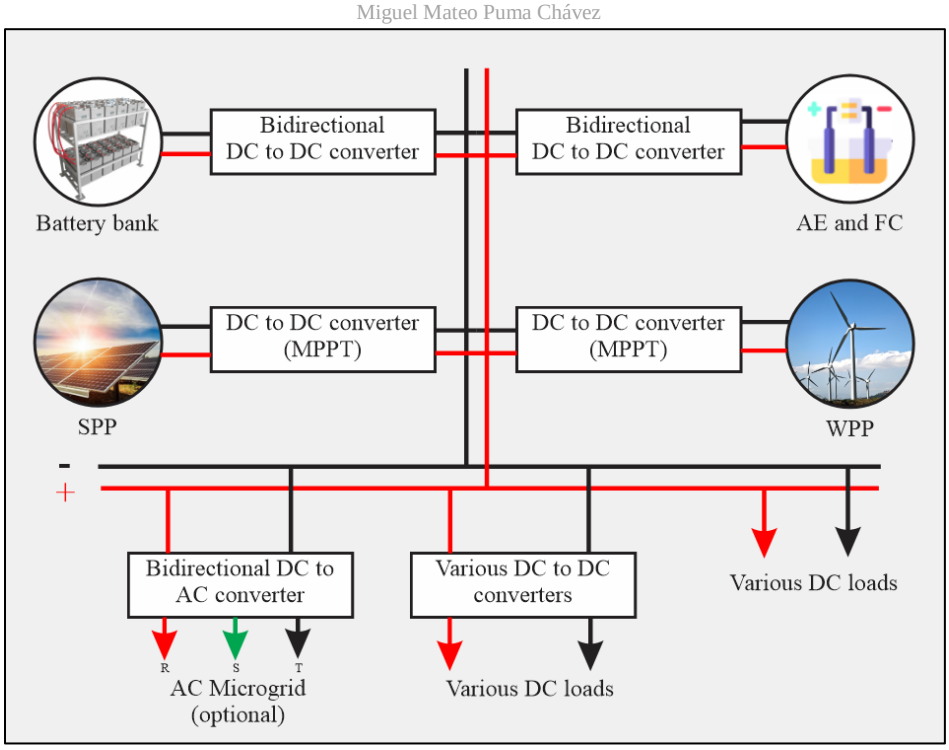

Figure 2: Conventional configuration of a DCMG.
Source: Own elaboration.

In order to reduce the number of individual converters and size of the system, the proposed configuration of DCMG by using a single multiport converter is depicted in Fig. 3. A bidirectional DC to DC circuit is employed to regulate the discharging and charging current of the battery bank, which is contingent upon the power disparity between the overall generation and load. Hence, two switches Q1 and Q2 are used to obtain bidirectional power flow of the battery bank. In order to consume power from DC bus during high generation as compared with load, AE is integrated through switch Q3. The FC needs to be supply load demand during steady state, hence switch Q4 is used which can be able to inject FC current into DC bus. Switches Q5 and Q6 are used to integrate WPP and SPP to DC bus as well as working as respective MPPT devices. Voltage at DC bus (Vdc) is obtained at output terminals of the multiport DC to DC converter.

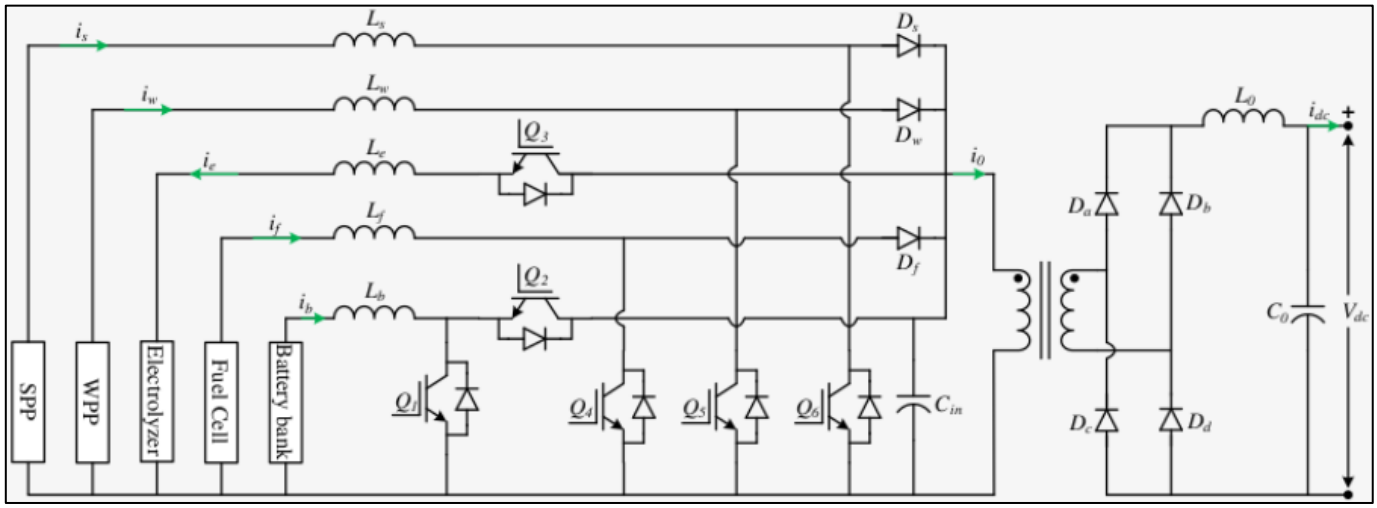

Figure 3: Proposed DCMG with multiport convert.
Source: Own elaboration.

III. MODELING OF VARIOUS COMPONENTS IN DCMG

Modeling of various components involved in proposed DCMG is prepared in this section. The PMSG is simulated utilizing an arbitrary d-q reference frame [10]. This paper presents a wind turbine's drive train model with improved accuracy, focusing on a two-mass system. The mechanical dynamics of the WPP are described by the following differential equations.

$$2B_t \frac{d\omega_t}{dt} = T_m - T_{sh} \quad (1)$$

$$\frac{1}{\omega_{elb}} \frac{d\theta_{tw}}{dt} = \omega_t - \omega_r \quad (2)$$

Aibi research, management and engineering journal. Volume 13, Number 2, May - August 2025, ISSN 2346-030X PP 1-11.

$$2B_g \frac{d\omega_r}{dt} = T_{sh} - T_g \quad (3)$$

Where, inertia constants of the turbine and PMSG are denoted by B_t and B_g respectively. θ_{tw} represents shaft twist angle, rotor speed of the PMSG is ω_r in p.u., angular speed of the turbine is denoted by ω_t in p.u., ω_{elb} represents electrical base speed. The shaft torque T_{sh} is

$$T_{sh} = R_{sh}\theta_{tw} + D_c \frac{d\theta_{tw}}{dt} \quad (4)$$

Where, R_{sh} is the shaft rigidity and D_c is the damping coefficient. Various coefficients of the drive train and wind turbine are listed in Table 1.

Table 1: Parameters of Wind system.

B_t (s)	4
B_g (s)	0.1
R_{sh} (p.u./electrical rad)	0.3
D_c (p.u./electrical rad)	0.7
Pole pairs	5
Armature resistance (Ω)	0.425
Magnetic flux linkage (Wb)	0.433
Inductance in stator (mH)	8.4
Operating torque (Nm)	40
Maximum power (KW)	6
Rated speed (rad/s)	153

Source: Own elaboration.

The implementation of a lead acid battery's electrochemical model is achieved with the assistance of [1]. The modeling is performed by employing a basic CVS with a consistent resistor, as depicted in Fig. 4. The CVS is characterized by equations (5) to (10).

$$V_m = V_{m0} - K_E(273 + \theta)(1 - SOC) \quad (5)$$

$$Q_e(t) = Q_{e\_init} + \int_0^t -I_m\tau \, d\tau \quad (6)$$

$$I_p = V_{PN}G_{P0} \exp\left(\frac{V_{PN}}{V_{P0}(\tau_P s+1)} + A_P\left(1 - \frac{\theta}{\theta_f}\right)\right) \quad (7)$$

$$C(I,\theta) = \frac{K_C C_0 K_t}{1+(K_C-1)\left(\frac{I}{I^*}\right)^\delta}, K_t = LUT(\theta) \quad (8)$$

$$SOC = 1 - \frac{Q_e}{C(0,\theta)}, DOC = 1 - \frac{Q_e}{C(I_{avg},\theta)} \quad (9)$$

$$\theta(t) = \theta_{init} + \int_0^t \frac{P_s - \frac{\theta-\theta_a}{R_\theta}}{C_\theta} d\tau \quad (10)$$

where, V_m and V_{m0} are the open-circuit voltage and open circuit voltage at full charge, θ is electrolyte temperature in ºC, Q_{e_init} is the initial extracted charge, I_m is the main branch current in A and Q_e is the extracted charge in Ampere seconds.

The 10 KW rating of the FC model has been developed by setting the operating voltage at 300 V, which the boost converter then converts to V_{dc}^*. The output voltage from the stack in the MATLAB simulation is subsequently linked to a controlled voltage source as illustrated in Fig. 5. The boost converter interfaces the FC dynamic model to the DC link. The paper examines the operating voltage of SOFC as 300 V, which is then boosted to 660 V by the boost converter. Important parameters of FC are listed in Table 2.

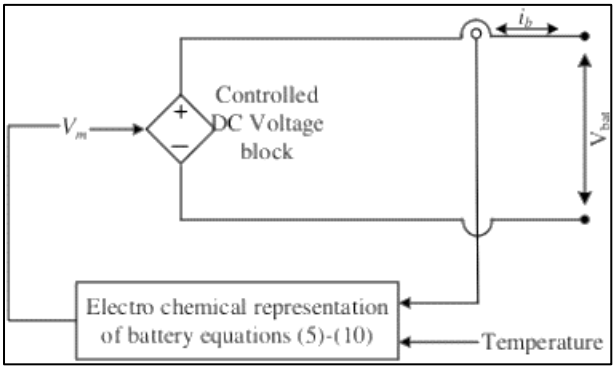

Figure 4: Lead acid battery's electrochemical model.
Source: Own elaboration.

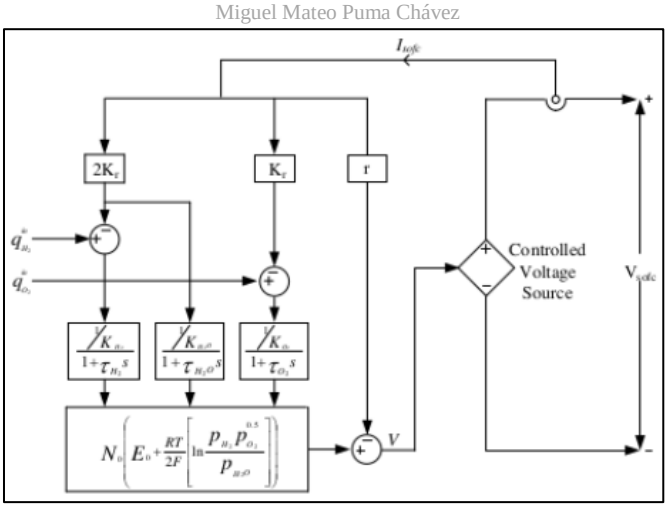

Figure 5: FC stack dynamic model.
Source: Own elaboration.

Table 2: Parameters of FC.

Absolute temperature (K)	1273
Faraday's value (C/mol)	96487
Number of cells in series in stack N_0	325
Constant $K_I=N_0/4F$ (Kmol/(A.s))	$0.842*10^{-6}$
Molar constant for H_2 (Kmol/(s.atm))	$8.43*10^{-4}$
Molar constant for H_2O (Kmol/(s.atm))	$2.81*10^{-4}$
Molar constant for O_2 (Kmol/(s.atm))	$2.52*10^{-3}$
H_2 response time flow τ_{H_2} (s)	26.1
H_2O response time flow τ_{H_2O} (s)	78.3
O_2 response time flow τ_{O_2} (s)	2.91
Ohmic loss (Ω)	$32813*10^{-8}$
Universal gas constant (J/Kmol.K)	8314

Source: Own elaboration.

The paper outlines the design of an AE rated at 10 KW while maintaining a current rating of 120 A. Consequently, the voltage across the AE is set to 86 V, the buck circuit is utilized to reduce the voltage from V_{dc}^{*} to 86 V.

The empirical current-voltage relationship can be utilized to model the kinetics of electrode reactions in an AE cell, which also incorporates a temperature parameter. The voltage of AE is denoted by the following equation:

$$V = nV_{rev} + \frac{r_1+r_2T}{A} I_e + (s_1 + s_2T + s_3T^2).\log(1 + \left(t_1 + \frac{t_2}{T} + \frac{t_3}{T^2}\right).(\frac{I_e}{A})) \quad (11)$$

Where, important parameters are: n that represents the number of cells, V_{rev} is the reversible cell potential, T is the temperature in ºC and I_e/A is the current density in A/m2.

The electrochemical AE model has been created in Simulink and linked to a buck converter through a CVS as illustrated in Fig. 6. Important parameters of AE are listed in Table 3.

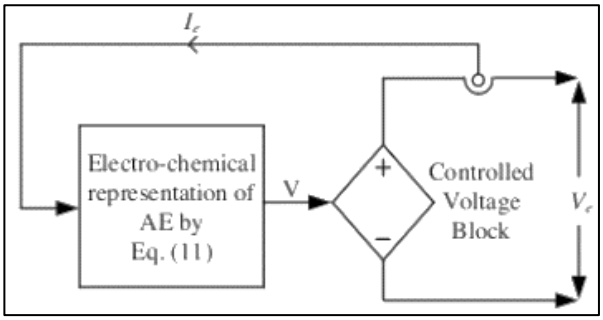

Figure 6: Aqua-electrolyzer model.
Source: Own elaboration.

Table 3: Parameters of Aqua Electrolyzer.

r_1 (Ω.m^2)	0.00015
r_2 (m^2.ºC^{-1})	-6.019*10^{-6}
s_1 (V)	2.427
s_2 (V.ºC^{-1})	-0.0307
s_3 (V.ºC^{-2})	3.9*10^{-4}
t_1 (A^{-1}.m^2)	0.214
t_2 (A^{-1}.m^2.ºC)	-9.87
t_3 (A^{-1}.m^2.ºC^2)	119.1
N	64
T (ºC)	70
A (cm^2)	873

Source: Own elaboration.

The modeling of PVS was examined by [2]. The modeling is conducted in (12), where I_{PV} and V_{PV} represent the current and voltage of the PVS respectively. The following equation is used to modeling the PVS:

$$I_{PV} = I_{ph} - I_0\left[\exp\left(\frac{q(I_{PV}R_s+V_{PV})}{AKT}\right)-1\right] - \frac{V_{PV}+I_{PV}R_s}{R_{sh}} \quad (12)$$

Where

$$I_{ph} = [I_{sc} + k(T - T_r)]\frac{G}{1000}$$

$$I_0 = I_{rr}[\frac{T}{T_r}]^3\exp(\frac{qV_{oc}}{AK}[\frac{1}{T_r} - \frac{1}{T}])$$

The design of MPPT of wind turbine is attempted by the following procedure, the wind turbine's power output is determined by the amount of power it captures.

$$P_t = \frac{1}{2}\rho A C_p(\lambda,\beta)v^3 \quad (13)$$

Where ρ is air density, A is blade's swept area, v is wind speed.

$$T_m = \frac{P_t}{\omega_t} \quad (14)$$

And $\lambda = \frac{\omega_t}{v}$

For MPPT operation $\lambda = \lambda_{opt} =$ constant,

$$\therefore \frac{\omega_{t_1}}{v_1} = \frac{\omega_{t_2}}{v_2} \quad (15)$$

Moreover, if wind turbine is operating under steady-state conditions with MPPT: C_p=constant=1 p.u.

$$\therefore T_m \propto \frac{v^3}{\omega_t} \quad (16)$$

By inserting (15) into (16) and calculating the torque ratio at two different wind speeds, we obtain:

$$\frac{T_{m1}}{T_{m2}} = \frac{v_1^3}{v_2^3}\frac{v_2}{v_1} = \frac{v_1^2}{v_2^2} \quad (17)$$

Similarly, MPPT of PVS is developed by using IC method.

IV. PROPOSED CONTROL METHOD OF DCMG

The STSM control possesses the capability to minimize chattering and is also resilient to changes in parameters [11]. The sample model of STSM controller is depicted in Fig. 7. The error signal is considered as ed in Fig. 7.

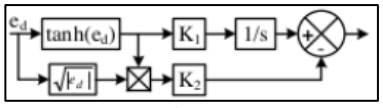

Figure 7: Sample of a STSM controller model.
Source: Own elaboration.

Well-designed STSM controllers are used while designing the proposed control method of the DCMG in place of conventional PI controllers. The combination of battery bank, FC and AE is considered to regulate voltage at DC bus since these are working as energy storage devices in the proposed DCMG. Hence, the error obtained from V_{dc} and its reference V_{dc}^* is given to both STSM controllers 1 and 2 to obtain reference hydrogen current I_h^* and battery current I_b^*. These are further compared with actual hydrogen current i_h and battery bank current i_b respectively

to produce required pulses for Q_1 to Q_4 by using hysteresis current controller loops. The boost converter switches of Q_5 and Q_6 are used to work as MPPT devices of PVS and wind system respectively.

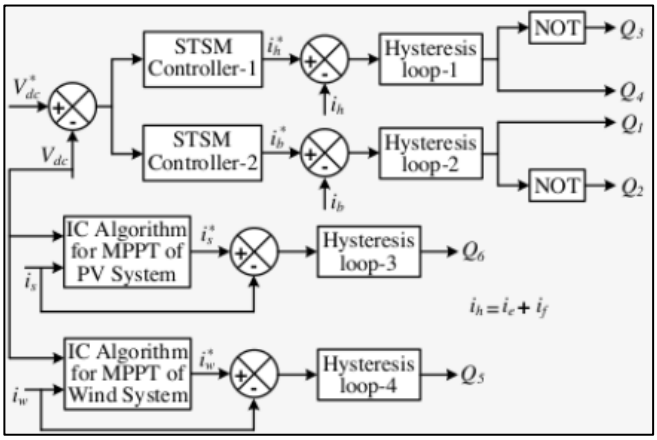

Figure 8: Proposed control method.
Source: Own elaboration.

V. RESULTS

To ensure optimal visualization, the results of different case studies will be presented using a single PVS and a single WPP. The HIL system has been designed to evaluate the effectiveness of the proposed approach outlined in this section. Two OPAL-RT devices are used to stablish the HIL configuration through appropriate connections.

The RTS has the capability to operate in real time and produce outcomes that closely resemble real life situations, considering different conditions. The HIL system is created by linking two OPAL-RT modules that have the capability to host the MATLAB model via a computer. The modules are connected in a loop by utilizing connecting cards. The plant is controlled by the computer housed in OPAL-RT unit 1; meanwhile, the proposed controller is set up within OPAL-RT unit 2. Fig. 9 illustrates the comprehensive laboratory configuration for the HIL model. The analog signals are transmitted from model of the dynamic plant to the unit controller. However, the proposed system's controller unit is transmitting digital signals to the plant. Various scenarios are being examined to showcase the efficiency and validate the functionality of the controller that has been suggested.

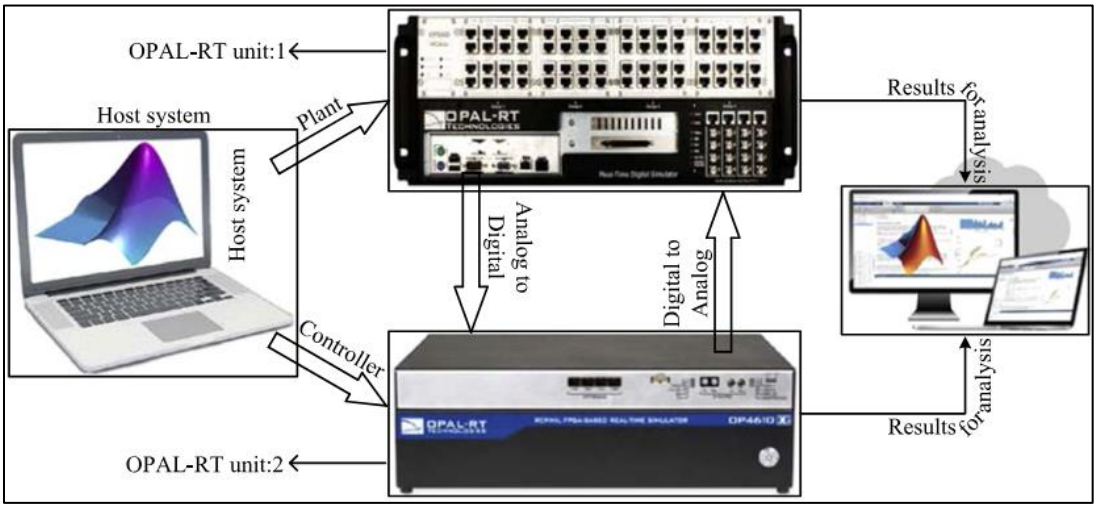

Figure 9: System diagram for the real-time simulation setup.
Source: Own elaboration.

Case A. Performance with AE

In order to assess the system's performance when operating with AE, the battery bank's SoC is assumed to have reached its maximum capacity, while also taking into account the availability of excess power from other sources. Based on the energy management system outlined in this document, the AE initiates the utilization of excess power as depicted in Fig. 10(a). Fig. 10(b) demonstrates the controlled response of the voltage at the DC bus, regulated by the buck converter of the AE.

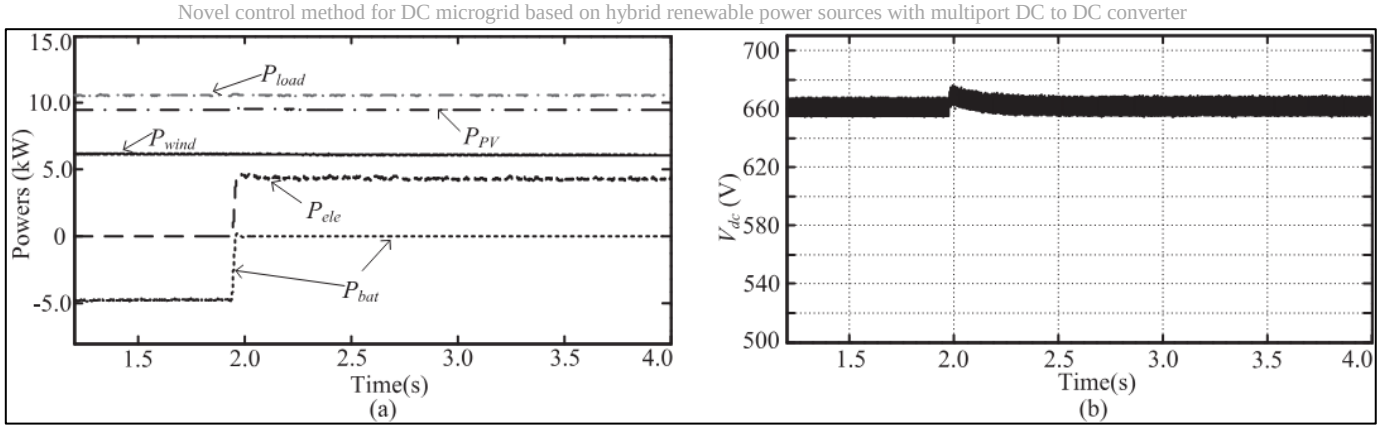

Figure 10: {Case A} (a) Powers, (b) Voltage.
Source: Own elaboration.

Case B. Performance with FC

The abrupt rise in power demand from 7.5 to 15 KW at t=10 sec. is being analyzed in this scenario to assess the DCMG's efficiency while being operated by FC. The battery in the energy management system will respond immediately to fulfill load requirements, while the fuel cell will gradually begin supplying power because of its slow dynamics. At approximately t=10.95 sec. the battery banks SoC decreases to 20%. The power supply from the DC stakes commences at t=11.16 sec. because of its sluggish dynamic characteristics and attains the required load at around t=12.8 sec. as shown in Fig. 11(a) during this procedure. Therefore, as the power supplied by the FC increases the power stored in the battery decreases until it reaches zero, at which point the FC supplies the entire required power in a stable condition. The proposed control scheme enables the attainment of intelligent coordination of this nature. The V_{dc} corresponding response is depicted in Fig. 11(b).

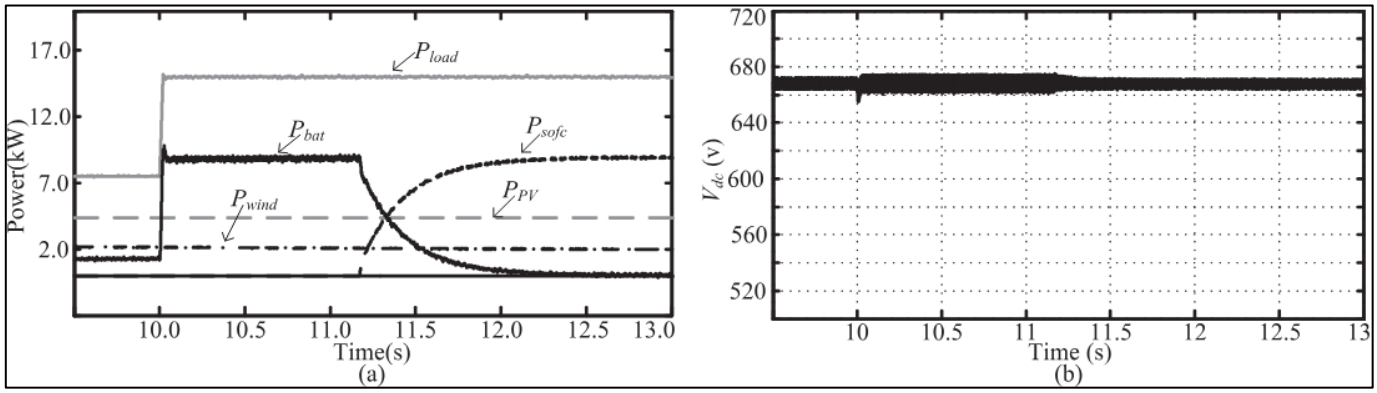

Figure 11: {Case B} (a) Powers, (b) Voltage.
Source: Own elaboration.

Case C. Performance under variations of meteorological changes

The evaluation of the DCMG's performance includes considering meteorological variations in weather patterns. The fluctuations in load, temperature, solar radiation, and wind velocity are considered as illustrated in Fig. 12. The different powers involved in this research paper are illustrated in Fig. 13. The AE, FC and battery bank are managing the equilibrium between total power production and load demand in the DCMG.

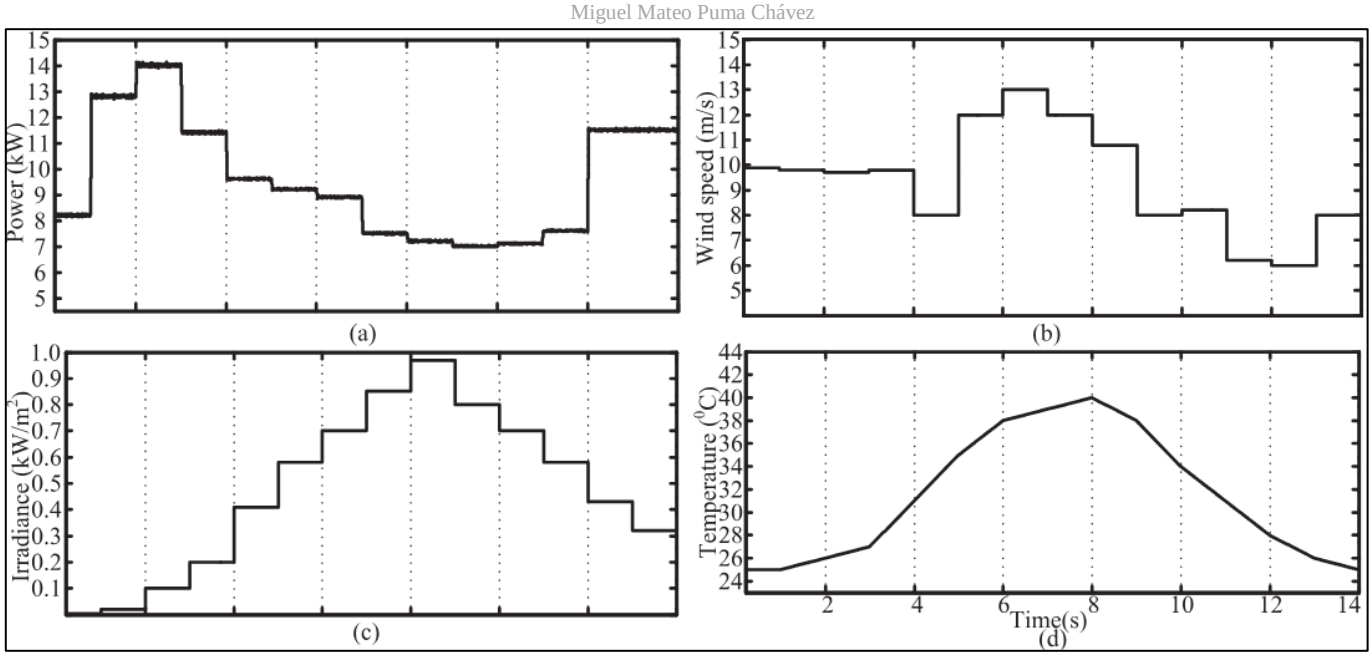

Figure 12: {Case C} Variation of (a) load, (b) wind speed, (c) irradiance and (d) temperature.
Source: Own elaboration.

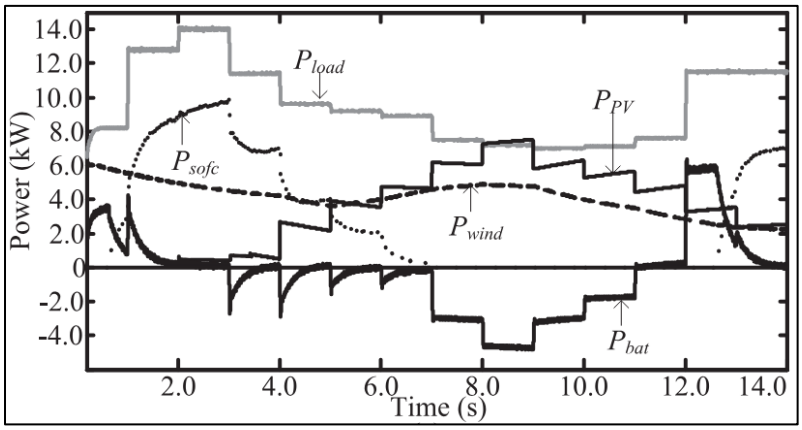

Figure 13: Powers in DCMG.
Source: Own elaboration.

Case D. Performance during changes in load and generation

Fig. 14(a) illustrates the powers of PVS, load, battery, FC and AE; taking into account various load changes. The data clearly shows that the battery is performing well and is responsive to sudden changes unlike FC and AE which are operating steadily. The AE transforms water into hydrogen and oxygen when the generation exceeds the load. In case of an abrupt surge in load, the battery initially discharges to stabilize the DC link voltage. Subsequently, either the AE or FC assumes control to sustain the voltage based on the power mismatch. The battery power reaches zero in a stable state, suggesting that a small battery bank is adequate. The voltage at the DC bus experiences notable fluctuations due to sudden changes in both the source and load. However, the variations in the DC bus voltage remain insignificant in comparison to the reference DC bus voltage of 660 V. Hydrogen pressures, production of hydrogen and voltage DC bus are shown in Fig.s 14(b), (c) and (d) respectively. The rapid responses observed were made achievable by the implementation of STSM controllers, which exhibit quick reactions to system changes.

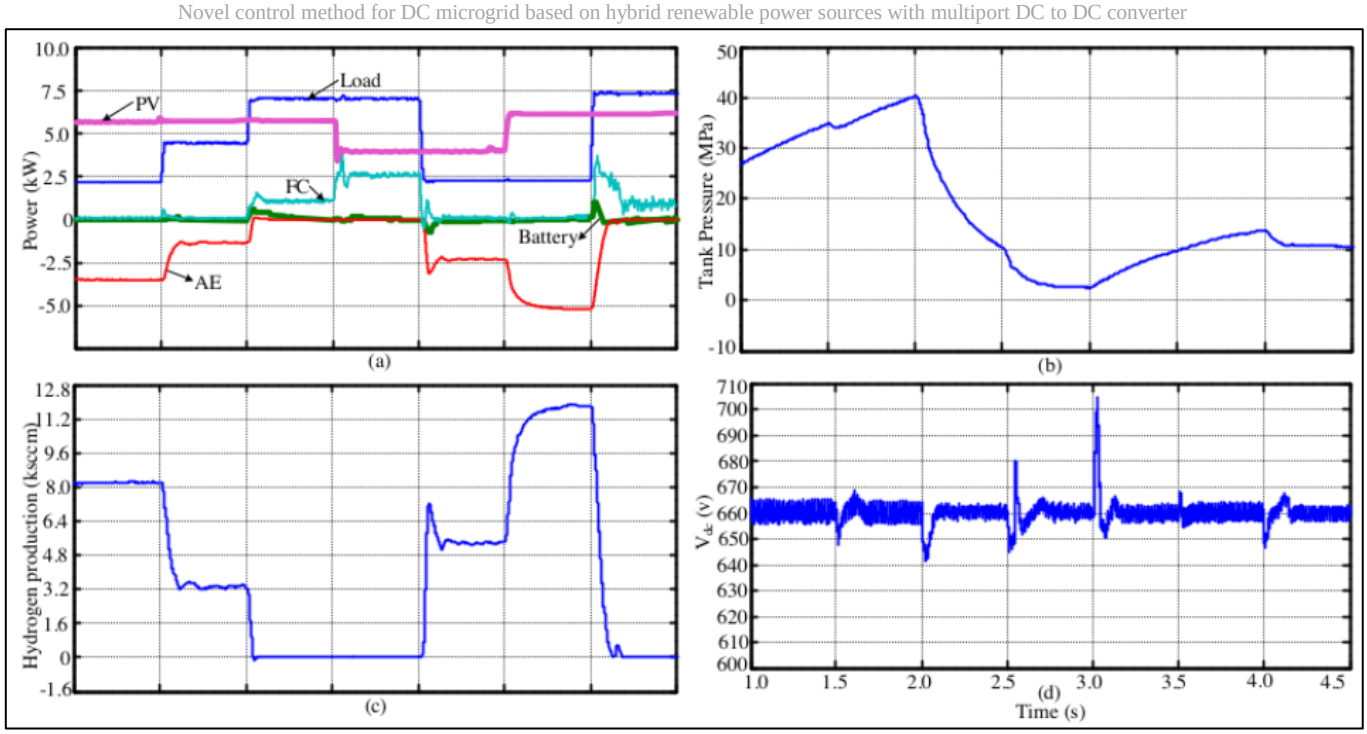

Figure 14: {Case D} (a) Powers, (b) tank pressure, (c) hydrogen production and (d) voltage.
Source: Own elaboration.

VI. CONCLUSIONS

The proposed DCMG along with control module with the help of STSM controllers is developed on multiport DC to DC converter. The proposed control methodology is simple and can allow connecting further power generating units to DCMG easily. The coordination between AE, battery and FC is obtained by using proposed control methodology. Various responses are obtained and analyzed by using HIL configuration with OPAL-RT modules in this paper. Validating results are obtained and satisfactory responses are presented in this paper.

VII. NOMENCLATURE

STSM: Super Twisting Sliding Mode
HIL: Hardware - in the - Loop.
RES: Renewable Energy Source.
AE: Aqua Electrolyzer.
FC: Fuel Cell.
WPP: Wind Power Plant.
PVS: Photovoltaic System.
DCMG: DC Microgrid.
PMSG: Permanent magnet synchronous generator
MPPT: Maximum Power Point Tracking.
IC: Incremental Conductance.
EMS: Energy Management System.
CVS: Controlled voltage source.
SPP: Solar Power Plant.
RTS: Real-time simulator
MATLAB: MATrix LABoratory Software
SOFC: Solid oxide fuel cell
STSM: Super-Twisting Sliding Mode
SoC: State of Charge

VIII.REFERENCES

[1] U. Chaithanya, K. Deepak, D. Besta, M. Khatoon, M. Samyuktha and P. Mounisha, "A Novel Control of DC to DC Converter for Renewable Energy Sources," 2023 International Conference on Innovative Data Communication Technologies and Application (ICIDCA), Uttarakhand, India, 2023, pp. 947-953, doi: 10.1109/ICIDCA56705.2023.10099786.

[2] Kandi Bhanu Prakash, "PV-Battery based standalone power supply system for rural applications", International Journal of New Technologies in Science and Engineering (IJNTSE), Vol. 8, Issue. 12, pp. 9-13, Dec. 2022.

[3] F. Barati, B. Ahmadi and O. Keysan, "A Hierarchical Control of Supercapacitor and Microsources in Islanded DC Microgrids," in IEEE Access, vol. 11, pp. 7056-7066, 2023, doi: 10.1109/ACCESS.2023.3237684.

[4] N. Hou, L. Ding, P. Gunawardena, T. Wang, Y. Zhang and Y. W. Li, "A Partial Power Processing Structure Embedding Renewable Energy Source and Energy Storage Element for Islanded DC Microgrid," in IEEE Transactions on Power Electronics, vol. 38, no. 3, pp. 4027-4039, March 2023, doi: 10.1109/TPEL.2022.3221349.

[5] R. Wang, W. Hassan, M. Negnevitsky and J. L. Soon, "Analysis and Experimental Verification of High-Efficiency DC-DC Converter for DC Microgrids," 2023 IEEE International Conference on Energy Technologies for Future Grids (ETFG), Wollongong, Australia, 2023, pp. 1-6, doi: 10.1109/ETFG55873.2023.10408536.

[6] A. Sheina, R. Zamora, X. Lin and A. M. Than Oo, "Protection and Control Strategy for Battery Energy Storage System in Islanded LV DC Microgrid Applications," 2023 IEEE Fifth International Conference on DC Microgrids (ICDCM), Auckland, New Zealand, 2023, pp. 1-6, doi: 10.1109/ICDCM54452.2023.10433611.

[7] Y. Zhang, "Analysis of High Gain DC-DC Converters for DC Microgrid," 2023 IEEE 3rd International Conference on Power, Electronics and Computer Applications (ICPECA), Shenyang, China, 2023, pp. 1354-1359, doi: 10.1109/ICPECA56706.2023.10075947.

[8] A. S. Shirodkar and C. Vyjayanthi, "Design and Development of Control Algorithm for a DC Microgrid System," 2023 IEEE 8th International Conference for Convergence in Technology (I2CT), Lonavla, India, 2023, pp. 1-6, doi: 10.1109/I2CT57861.2023.10126209.

[9] U. Hussan et al., "Smooth and Uninterrupted Operation of Standalone DC Microgrid Under High and Low Penetration of RESs," in IEEE Access, vol. 12, pp. 48620-48629, 2024, doi: 10.1109/ACCESS.2024.3374209.

[10] Koilada Rajesh, "Novel Control of Boost Converter for MPPT of Wind Turbine", International Journal of New Technologies in Science and Engineering (IJNTSE), Vol. 8, Issue. 6, pp. 1-6, June. 2022.

[11] C. Mu, C. Sun, C. Qian and R. Zhang, "Super-twisting sliding mode control based on Lyapunov analysis for the cursing flight of hypersonic vehicles," 2013 10th IEEE International Conference on Control and Automation (ICCA), Hangzhou, China, 2013, pp. 522-527, doi: 10.1109/ICCA.2013.6565017.

[12] M. M. Puma-Chávez, Python y Energías Renovables: Innovaciones en Ingeniería Eléctrica, 1st ed. 2025, pp. 16–18. ISBN: 9798308253341. Available: https://www.amazon.com/dp/B0DV5B5J2M.

[13] E. Agnoletto, D. Castro, R. Neves, R. Machado, & V. Oliveira, "An optimal energy management technique using the ϵ-constraint method for grid-tied and stand-alone battery-based microgrids", IEEE Access, vol. 7, p. 165928-165942, 2019, doi: 10.1109/access.2019.2954050.

[14] G. Liu, B. Ollis, M. Ferrari, A. Sundararajan, & K. Tomsovic, "Robust scheduling of networked microgrids for economics and resilience improvement", Energies, vol. 15, no. 6, p. 2249, 2022, doi: 10.3390/en15062249.

[15] Y. Xiong, L. Chen, T. Zheng, S. Yang, & S. Mei, "Electricity-heat-hydrogen modeling of hydrogen storage system considering off-design characteristics", IEEE Access, vol. 9, p. 156768-156777, 2021, doi: 10.1109/access.2021.3130175.

[16] N. Mlilo, J. Brown, & T. Ahfock, "Impact of intermittent renewable energy generation penetration on the power system networks – a review", Technology and Economics of Smart Grids and Sustainable Energy, vol. 6, no. 1, 2021, doi: 10.1007/s40866-021-00123-w.

[17] Y. Wang, Y. Qin, Y. Wang, Z. Ma, Z. Zhao, & Y. Wang, "Integrated energy system operation considering building thermal inertia and hydrogen storage systems", Sustainable Energy & Fuels, vol. 7, no. 18, p. 4654-4667, 2023, doi: 10.1039/d3se00549f.

[18] O. Utomo, M. Abeysekera, & C. Ugalde-Loo, "Optimal operation of a hydrogen storage and fuel cell coupled integrated energy system", Sustainability, vol. 13, no. 6, p. 3525, 2021, doi: 10.3390/su13063525.

[19] G. Chicco, S. Riaz, A. Mazza, & P. Mancarella, "Flexibility from distributed multienergy systems", Proceedings of the IEEE, vol. 108, no. 9, p. 1496-1517, 2020, doi: 10.1109/jproc.2020.2986378.

[20] T. Wen, Z. Zhang, X. Lin, Z. Li, C. Chen, & Z. Wang, "Research on modeling and the operation strategy of a hydrogen-battery hybrid energy storage system for flexible wind farm grid-connection", IEEE Access, vol. 8, p. 79347-79356, 2020, doi: 10.1109/access.2020.2990581.

[21] R. Khezri and A. Mahmoudi, "Review on the state-of-the-art multi-objective optimisation of hybrid standalone/grid-connected energy systems", Iet Generation Transmission & Distribution, vol. 14, no. 20, p. 4285-4300, 2020, doi: 10.1049/iet-gtd.2020.0453.